sciendo
Acta hort regiotec, 24, 2021(1): 28–48
DOI: 10.2478/ahr-2021-0022

Research Article

Numerical assessment of climate change impact on the hydrological regime of a small Mediterranean river, Lesvos Island, Greece

Eleni Ioanna Koutsovili[1]*, Ourania Tzoraki[1], Nicolaos Theodossiou[2], Petros Gaganis[3]
[1]*University of the Aegean, Department of Marine Sciences, Mytilene, Greece*
[2]*Aristotle University of Thessaloniki, Department of Civil Engineering, Thessaloniki, Greece*
[3]*University of the Aegean, Department of Environment, Mytilene, Greece*

Article Details: Received: 2021-02-22 | Accepted: 2021-03-31 | Available online: 2021-05-31

© 2021, Eleni Ioanna Koutsovili, Ourania Tzoraki, Nicolaos Theodossiou, Petros Gaganis
This is an open access article licensed under the Creative Commons Attribution-NonCommercial-NoDerivs License (http://creativecommons.org/licenses/by-nc-nd/4.0/)

SCREENED BY iThenticate® Professional Plagiarism Prevention

Frequency of flash floods and droughts in the Mediterranean climate zone is expected to rise in the coming years due to change of its climate. The assessment of the climate change impact at a basin scale is essential for developing mitigation and adaptation plans. This study analyses the variation of the hydrologic regime of a small Mediterranean river (the Kalloni river in Lesvos Island, Greece) by the examination of possible future climate change scenarios. The hydrologic response of the basin was simulated based on Hydrologic Modeling System developed by the Hydrologic Engineering Center (HEC-HMS). Weather Generator version 6 from the Long Ashton Research Station (LARS-WG 6.0) was utilized to forecast climate data from 2021 to 2080. These forecasted climate data were then assigned as weather inputs to HEC-HMS to downscale the climate predictions of five large-scale general circulation models (GCMs) for three possible emission scenarios (such as RCP 2.6, RCP 4.5, and RCP 8.5). The alteration of the Kalloni hydrologic regime is evaluated by comparing GCMs based estimates of future streamflow and evapotranspiration with business as usual (BaU) scenario. Variation was noted in seasonal and in annual scale forecasting of long-term average discharges, which show increasing trend in autumn and decreasing in summer and there is observed a general upward trend of actual evapotranspiration losses.

Keywords: climate change, hydrological regime, HEC-HMS model, GCMs, LARS-WG 6.0

1 Introduction

Water resources management and the design of flood prevention and adaptation strategies are becoming more challenging due to the uncertainties of climate change (Refsgaard et al., 2013). Global warming, variations in precipitation, and changes in the frequency of extreme events increase the probability of flood occurrences and change the total and seasonal water supply, among other impacts (Parry et al., 2007). Projections by the fifth iteration of the Intergovernmental Panel on Climate Change (IPCC) point towards a likely decrease in precipitation over the Mediterranean by 30–45%, especially if temperature rises by 1.4 °C (Cisneros, 2014; Zhai et al., 2018). Consequently, the frequency of flash floods and droughts in the region is expected to increase in the coming years, seriously altering the ecological and hydrological patterns of river basins (Tzoraki, 2020).

Addressing of climate change effects in the development of hazardous risk adaptation and mitigation plans has been on the agenda of many governments and institutions (Lavell et al., 2012). Hence, effective planning requires the examination of both current and projected climate change scenarios (Shrestha at al., 2017). According to IPCC, GCMs are advanced tools currently available for simulating the response of global climate system to increasing greenhouse gas concentrations. The use of GCMs has been the most crucial method for studying the implications of climate change (Wu et al., 2015). In a global scale, several studies have quantified potential changes in hydrological dynamics of river basins by climate change projections on the basis of GCMs (i.e., Sharafati et al., 2020; Ismail et al., 2020; Ebrahim et al., 2012; Hajian et al., 2016; QIN & LU, 2014; Emam et al., 2016; Yilmaz & Imteaz, 2011). The findings of these studies indicate that hydrological processes are highly sensitive to precipitation and temperature. Therefore, climate change can have a significant effect on hydrological regime of a river basin (Sharafati et al., 2020).

***Corresponding Author:** Eleni Ioanna Koutsovili. University of the Aegean, Environment School, Department of Marine Sciences, 81100 Mytilene, Greece; e-mail: mard18001@marine.aegean.gr

Although GCMs are very important tools for studying the implications of climate change, these contain biases when compared to observed data due to their parameterization systems and large grid size (Sharma et al., 2007). Outputs from the GCMs are typically defined at 250–600 km grids which are quite coarse relative to the scale of exposure units in most regional impact assessments. In fact, hydrological studies dealing with climate change impacts on small basins are particularly challenging, as they may require rainfall and temperature data at spatial resolution of 1 km^2 (Shrestha et al., 2017). In order to overcome this problem, many different downscaling methods have been developed over the last few decades (Ebrahim et al., 2012). These methods aim to provide sufficient hydrological variables by downscaling large-scale GCMs forecasts to a local scale (Ebrahim et al., 2012). Subsequently, the generated variables can be used as inputs to basin-scale hydrological models to predict climate-induced changes in flow patterns. There is a range of different downscaling techniques, which are mainly dynamical downscaling, statistical downscaling, regression based downscaling, weather typing procedure and the stochastic weather generator (Semenov & Barrow, 1997; Wilby et al., 2002; Sunyer et al., 2012; Shrestha et al., 2017). The most commonly applied are dynamic and statistical downscaling methods (Shrestha et al., 2017). Dynamic downscaling is based on high-resolution regional climate models combined with observations and output from lower-resolution larger-scale climate models, while statistical downscaling is based on the development and application of statistical relationships between local weather variables and large-scale predictors (Wilby et al., 2002; Hewer & Gough, 2018; Nourani et al., 2018; Sharafati et al., 2020). Additional, weather generators have been used successfully for downscaling the output of the GCMs over different regions (Sharafati et al., 2020). Weather Generator developed by the Long Ashton Research Station (LARS-WG) has been widely used to assess possible effects of climate change on hydrological processes (Sharafati et al., 2020). However, uncertainties associated with simulating various response mechanisms in GCMs are responsible for the fact that GCMs may simulate quite different responses to the same forcing (Randall et al., 2007). These differences are unlikely to be consistent with the uncertainty range of regional projections. Despite considerable improvements in computational power in recent years, climate models do not guarantee a representative range at finer scales of drainage systems (Shrestha et al., 2017).

Future greenhouse gas emission scenarios are appropriate tools for analyzing the influence on future emission outcomes due to various driving forces and assessing related uncertainties (IPCC, 2000). The IPCC defined a series of Representative Concentration Pathway (RCP) emission scenarios for future climate projections based on the Coupled Model Intercom Paring Project phase 5 (CMIP5). These scenarios are based on different 21st century pathways of greenhouse gas (GHG) emissions, population, and socio-economic conditions (IPCC, 2014). The RCPs include a stringent mitigation scenario (RCP2.6), two intermediate scenarios (RCP4.5 and RCP6.0), and one scenario with very high GHG emissions (RCP8.5) (IPCC, 2014). These various climate change scenarios can be used to define the climate change impact on hydrological processes, by downscaling the large-scale GCMs predictions to local scale with the LARS-WG (Sharafati et al., 2020).

The main objective of the current study is the numerical evaluation of climate change impact (2021–2080) on the hydrological regime of a smal Mediterranean river, the Kalloni river, which flows over Lesvos Island of Greece. The river basin is of significant importance due to high biodiversity richness of its NATURA 2000 areas. The developed approach based on the integration of spatial downscaling of GCMs and hydrological simulation has been adopted in the study.

2 Material and methods

A methodological framework summarized in Fig. 1 was developed in the study to assess climate change effects on the hydrology of the Kalloni river basin. Climate change impacts on the basin hydrology were evaluated by comparing GCMs based estimates of future streamflow and evapotranspiration with business as usual (BaU) or baseline scenario.

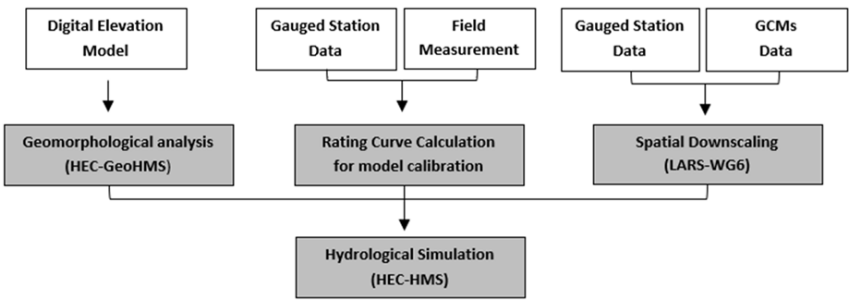


Figure 1 Flow diagram of methodological framework



Figure 2 Kalloni river basin in Lesvos Island, Greece

2.1 Study area

The Kalloni river basin illustrated in Fig. 2, which occupies the area of 40.28 km^2 was considered for the current study. The basin drains the wider area of the Kalloni settlement which is the second largest commercial centre of Lesvos Island. Its hydrographic network, with the total length of 34.92 km, is characterized as a dendritic type with many ephemeral streams. The basin area varies from lowland to mountainous in nature (Fig. 3a). North-western and western parts are mountainous areas with altitude reaching 690.3 m. North-eastern and central parts are intermediate hilly, of an average altitude of 300 m. The southern part is a large plain with an altitude almost equal to mean sea level. Main economic activities in the area are agriculture, livestock, and small local businesses. Fig. 3b shows that the watershed is primarily covered by agriculture (olive groves and cultivation patterns). Moreover, there are some small pine and oak forests at the northern tip of the basin, brushland habitats at the east and some artificial surfaces. Finally, in the southern part of the basin at the mouth of the torrent, wetlands and swampy areas develop. Land use data are provided by the Decentralized Administration of the North Aegean.

The study area has a Mediterranean climate with warm, dry summers and cool, mild, rainy winters (HMSO, 1962). More specifically, the average annual temperature is approximately 17 °C, with an average minimum temperature of 12.2 °C and an average maximum temperature of 21.4 °C. The mean annual rainfall depth over the Kalloni river basin is 514 mm, ranging from a daily minimum of 2.1 mm in summer (July) to a maximum of 98.5 mm in winter (January). Historical weather data from 2003 to 2020 in terms of daily precipitation, maximum and minimum temperature, solar radiation, relative humidity, and wind speed were collected from the Agia Paraskevi Meteorological Station. Water level data was obtained from automatic hydrometric station operating in Kalloni bridge. The river velocity and level were measured by field work to construct the rating curve.

In recent years, extended periods of drought are followed by sudden rainfalls of high intensity and short duration. This results in large volumes of water, which are not properly absorbed by the soil, ending up in the urban fabric. At the same time, the reduced cross-section of the riverbed at this point leads to overflow of the river with hazardous consequences for the infrastructures and the inhabitants. As a result, Kalloni experienced significant floods in 1986, 2005, 2011, 2016 (Matrai & Tzoraki, 2018).

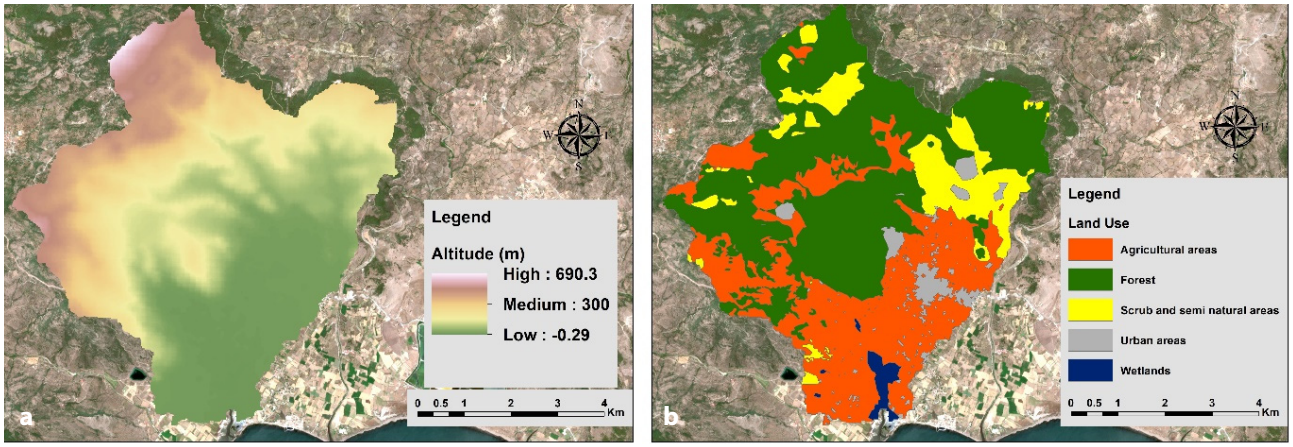


Figure 3 (a) Altitude and (b) Land uses of basin area

2.2 Geomorphological analysis

Analyses of geomorphological and hydrological characteristics of the study area were performed through HEC-GeoHMS extension of ArcMap and ArcHydro toolbox. HEC-GeoHMS extension was developed as a geospatial hydrology toolkit for engineers and hydrologists. The program allows users to visualize spatial information, document watershed characteristics, delineate subbasins and streams, and expediently create hydrologic inputs for Hydrologic Modeling System version 4.3 developed by the Hydrologic Engineering Center (HEC-HMS) (USACE, 2013). More specifically, HEC-GeoHMS produces a background map file and a basin model file as inputs to HEC-HMS. The map file visualizes basin's subbasins and watercourses of the study area, and the basin model file contains hydrological and geomorphological elements of the basin.

A digital elevation model (DEM) with 25 m grid from the European Environmental Agency was used as an input in HEC-GeoHMS to derive eight additional datasets that collectively describe drainage pattern of the watershed. The first step is to fill the sinks from the raw DEM and then use it as an input to delineate the Kalloni stream network and the watershed boundary. The produced datasets consist of five grid layers that represent the flow direction, flow accumulation, stream definition, stream segmentation, and watershed delineation, and two vector layers of the watershed and streams. Various stages of watershed generation in HEC-GeoHMS are shown in Figs 4, 5 and 6. Therefore, twenty-three subbasins and corresponding reaches are identified within the Kalloni basin area.

2.3 Rating curve calculation with field measurements

River monitoring is a critical issue for hydrological modeling that relies strongly on the use of flow rating curves (Manfreda, 2018). Rating curves define stage-discharge relationship and are usually developed by making frequent direct discharge measurements at stream gauging stations. Moreover, rating curves depend on the hydraulic characteristics of the stream channel and floodplain. Hence, they may vary over time in alluvial rivers, as river-bed characteristics change over time (Westerberg et al., 2011). This implies the need for frequent and time-consuming field survey.

In this study, field work measurements were carried out at characteristic cross sections of the streams aiming at calculating rating curves. The equipment consisted of a small flow meter device with a propeller, which is a portable flow measurement system in rivers, open canals or even in open water pipes. The rating curve

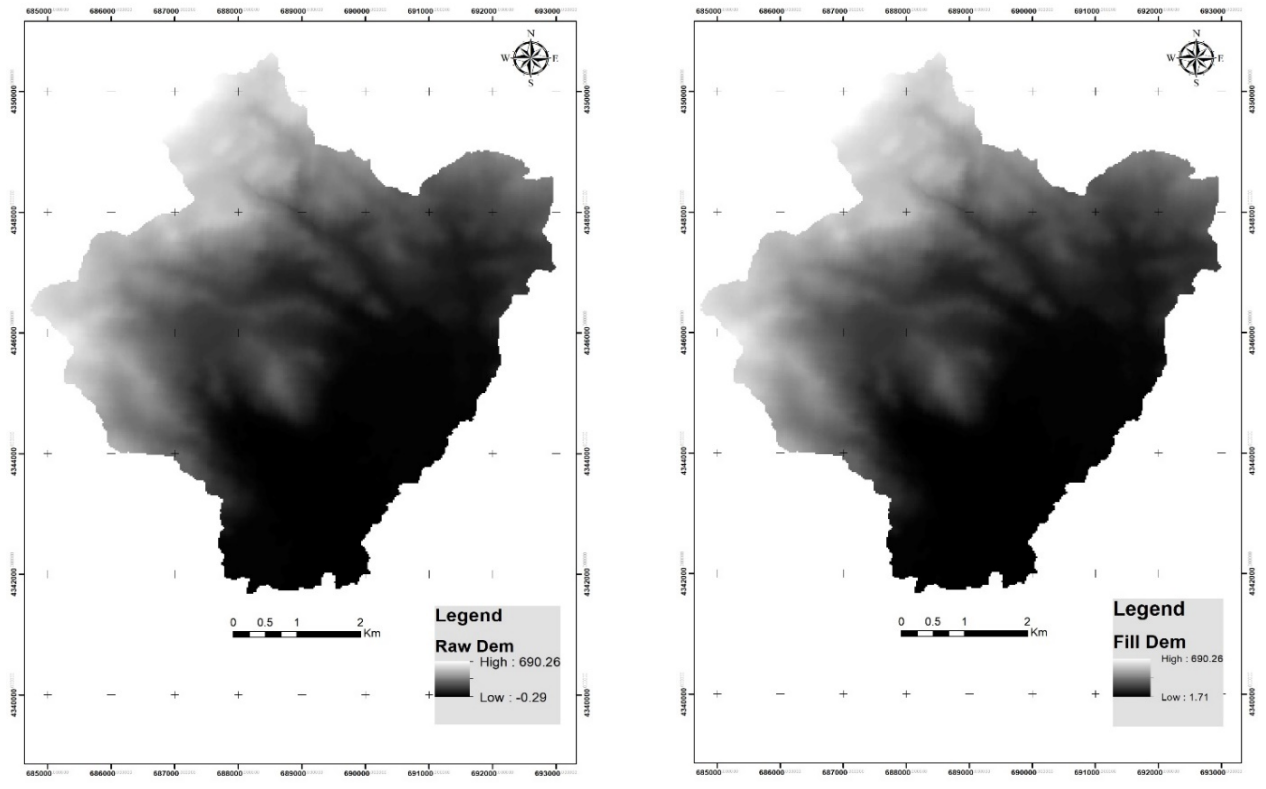


Figure 4 Kalloni raw DEM and fill DEM produced in HEC-GeoHMS

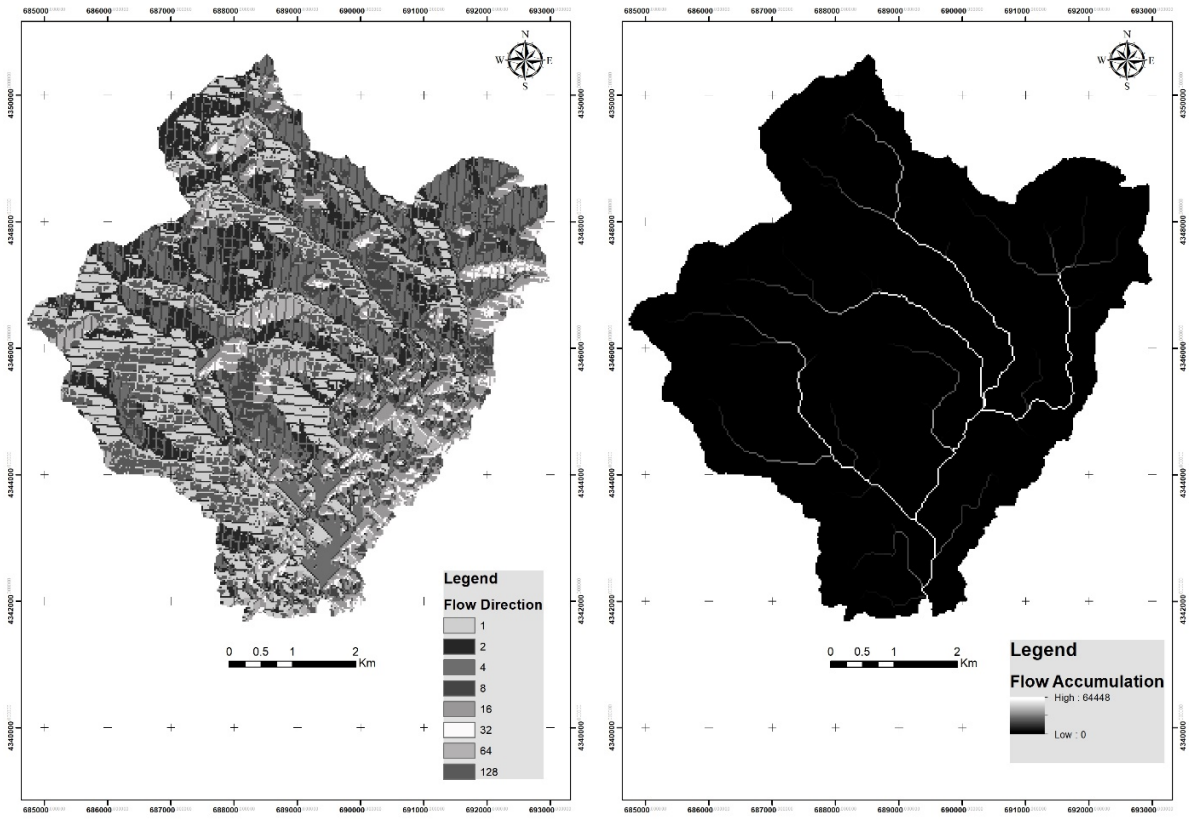


Figure 5 Flow direction and flow accumulation maps generated in HEC-GeoHMS

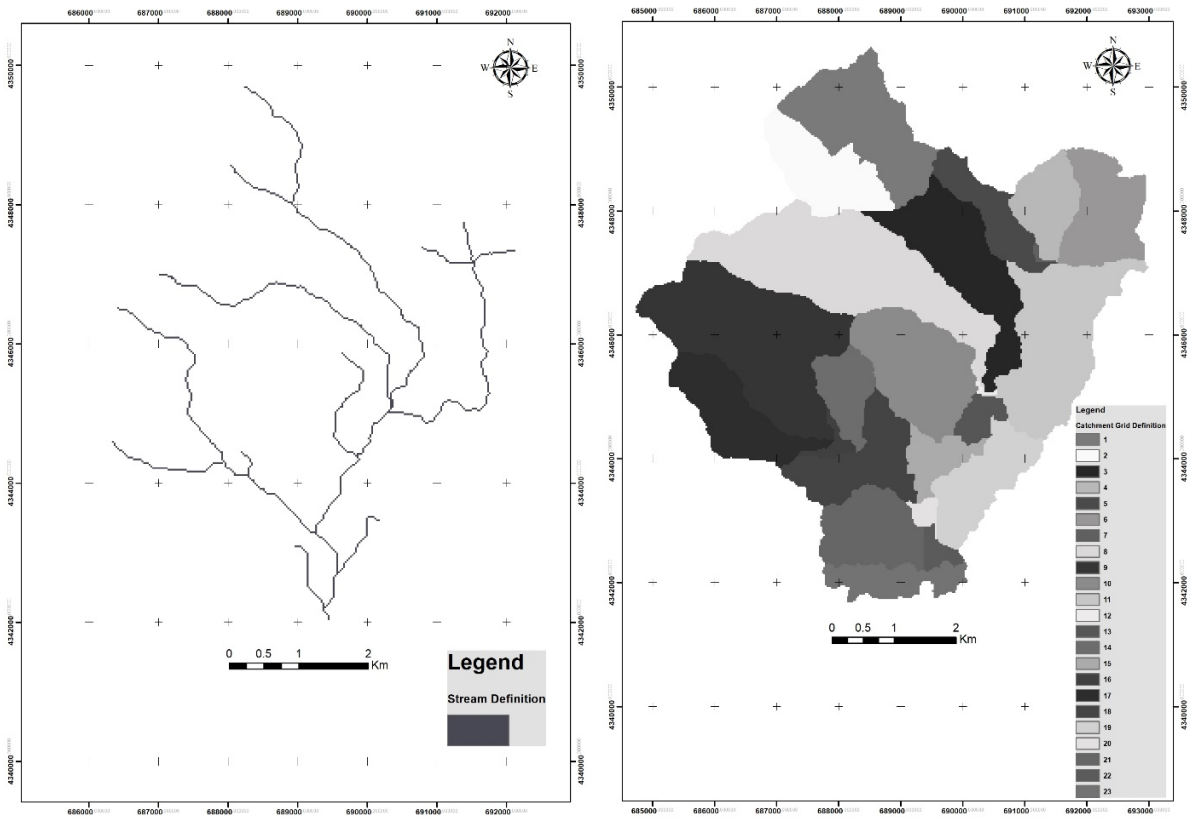


Figure 6 Stream network and watershed generation in HEC-GeoHMS

equation for discharge (Q) and stage (H) was calculated as follows:

$$Q = 2.7837 \times H^{1.1608} \quad (2.1)$$

Subsequently, the observed flow time series generated by the rating curve are used to calibrate the hydrological model HEC-HMS for time period 2018–2019. Each observed value of daily discharge was estimated from the rating curve equation using observed daily stage measured in real time by a telemetric station operating in Kalloni since 2018.

2.4 Spatial downscaling of large-scale climate predictions

Weather Generator version 6.0 from the Long Ashton Research Station (LARS-WG 6.0) is a single site numerical model for generating daily time-series of climate variables, namely, precipitation (mm), maximum and minimum temperature (°C), and solar radiation ($MJm^{-2}.day^{-1}$). LARS-WG 6.0 is suitable for downscaling coarse resolution climate model simulations in local spatial scale for different climate change scenarios (Sharafati et al., 2020). The model, after calibrating site parameters with observed weather data for the baseline period, is capable of simulating synthetic daily time series of weather data that are statistically similar to the observed weather (Wilks & Wilby, 1999). LARS-WG 6.0 uses a semi-empirical distribution to calculate the length of wet and dry days (Racsko et al., 1991). Moreover, it considers each weather variable as a stochastic variable, and simulates seasonal cycles through Fourier series (Sharafati et al., 2020).

Methodology for spatial downscaling using LARS-WG to generate future climate data can be divided into three major steps: model calibration (Site Analysis), model validation (QTest), and generation of synthetic weather data (Generator). Parameter files derived during the model calibration step are used to generate synthetic weather data having the same statistical characteristics as the original observed data but differing on a daily basis. In order to ensure that the simulated data probability distributions are close to the true long-term observed distributions, a model validation process must be performed. The QTest validation option of LARS-WG carries out a statistical comparison of generated and observed weather data using the Kolmogorov-Smirnov (K-S) test, the *T*-test, and the *F*-test. Once LARS-WG has been calibrated and the performance of the weather generator has been verified, synthetic weather data may be simulated using the Generator option. This option may be used to generate synthetic data which have the same statistical characteristics as the observed weather data (baseline scenario), or to generate synthetic weather data corresponding to a climate change scenario from GCMs (Semenov & Barrow, 2002).

The current version LARS-WG 6.0 generates high resolution climate change scenarios over a region using direct outputs from General Circulation Models (GCMs). LARS-WG 6.0 incorporates projections from five GCMs with the different climate scenarios RCP2.6, RCP4.5, and RCP8.5 used in the IPCC. Table 1 summarizes the different GCMs and RCPs that are taken into consideration in this study to forecast futuristic climate data for a period of 60 years from 2021 to 2080. Calibration of site parameters is performed for baseline period of 18 years from 2003 to 2020.

2.5 Hydrological simulation and calibration

Hydrologic Engineering Centre's Hydrologic Modeling System (HEC-HMS) was designed by the United States Army Corps of Engineers (USACE) as a software tool for simulating complete hydrological cycle in the context of solving engineering problems (Scharffenberg et al., 2010). HEC-HMS is a deterministic, semi-distributed, conceptual model which is designed to simulate precipitation-runoff processes of dendritic drainage basins. It is applicable to a wide range of geographic areas for solving the widest possible range of problems (USACE, 2013). The software has been applied in a wide variety of geographical regions, such as large river basins, and small municipal and natural watersheds. In addition, depending on objectives of the study, it can be applied

Table 1 Summary of the five GCMs and corresponding emission scenarios (RCPs)

GCM	Institution	Grid Resolution	RCP
EC-EARTH	European community Earth-System Model	1.125° × 1.125°	RCP4.5, RCP8.5
GFDL-CM3	NOAA Geophysical Fluid Dynamics Laboratory	2° × 2.5°	RCP4.5, RCP8.5
HadGEM2-ES	Met Office Hadley Center, United Kingdom	1.25° × 1.875o	RCP2.6, RCP4.5, RCP8.5
MIROC5	Atmosphere and Ocean Research Institute (The University of Tokyo), National Institute for Environment Studies and Japan Agency for Marine-Earth Science and Technology, Japan	1.40° × 1.41°	RCP4.5, RCP8.5
MPI-ESM-MR	Max Planck Institute for Meteorology, Germany	1.85° × 1.875°	RCP4.5, RCP8.5

for simulation of either individual events or continuous large-scale events.

HEC-HMS has been widely used all over the world in a number of studies, including flood forecasting (Verma et al., 2010), land use change impacts (Ali et al., 2011), and also assessing the impact of climate change. Nyaupane et al. (2018) used HEC-HMS for prediction of future peak flow condition in the Irwin Creek watershed located in Charlotte, North Carolina. The study highlighted the significance of consideration of climate change as a factor likely to result in increased peak discharge in the existing urban watersheds. The hydrologic impacts of climate change in the Tungabhadra river basin in India was also assessed by Meenu et al. (2012). They utilized the HEC-HMS to model hydrologic processes and the Statistical Down Scaling Model (SDSM) to downscale daily precipitation, and maximum and minimum temperature. Moreover, Bai et al. (2019) proposed a framework combining HEC-HMS and the Coupled Model Intercomparison Project Phase 5 (CMIP5) GCMs to assess the impact of climate change on flood events in the Nippersink Creek watershed located in Northeastern Illinois. They found that the increase in greenhouse gas concentration under RCP 8.5 scenario can increase future precipitation. It may induce a greater impact on flood events by 110% increase from historically-observed 100 year return period flood.

Each model run incorporates a basin model describing basin's connectivity and physical characteristics, a meteorological model storing the precipitation and evapotranspiration data, and a control specification with run options to attain outcomes (Verma et al., 2010). In HEC-HMS, a basin model is constructed by dividing the hydrological cycle (evaporation, surface runoff, infiltration, and groundwater recharge) into individual parts with possibility of processing each one separately. Therefore, each component of the hydrological cycle is represented by a mathematical model. HEC-HMS also provides supplemental analysis tools for model optimization, forecasting streamflow, depth-area reduction, assessing model uncertainty, erosion and sediment transport, and water quality (Wang et al., 2016). Furthermore, spatial data sets can be organized in GIS platforms using HEC-GeoHMS, and then directly imported into HEC-HMS (Ali et al., 2011).

In the present study, hydrological simulation is performed in the examined basin with a daily time step. For infiltration loss calculation of the watershed, the "deficit and constant" method is implemented. The deficit and constant loss model uses a single soil layer to account for continuous changes in moisture content (US Army Corps of Engineers, 2008). In addition, the "Clark unit hydrograph" method is used to transform the flows and calculate the direct runoff from excess precipitation. The runoff is considered to be through a linear reservoir. Furthermore, the "linear reservoir" method is used to account the baseflow. The central idea of the method is to take into account an underground reservoir charged during the infiltration phase of rainwater and then discharged, contributing to the surface flow after the end of the rainfall. Finally, the "Lag" method is selected as the channel routing model. Table 2 summarizes the calculation methods for all the components of the HEC-HMS model applied in the present study.

Table 2 Calculation methods for components of the basin and meteorological models

Component	Calculation method
Canopy	simple canopy
Loss	deficit and constant
Transform	clark unit hydrograph
Baseflow	linear reservoir
Routing	lag
Evapotranspiration	constant monthly

The inclusion of the evapotranspiration process in the HEC-HMS model is significant for long-term simulations, and it is also necessary when using the deficit and constant loss method. In the case of the Kalloni, the method of constant monthly evapotranspiration is selected, which requires a potential monthly evaporation rate (mm. month^{-1}) and a crop coefficient from all subbasins. The modified Blaney-Criddle method is applied to calculate the mean daily potential evapotranspiration for each month (Doorenbos & Pruitt, 1977):

$$ETd = a + b \times p \times (0.46 \times T + 8.16) \qquad (2.2)$$

where:
ETd – the daily potential evapotranspiration (mm.d^{-1}); T – the average monthly temperature (°C); p – the mean daily percentage of annual daytime hours (%), and a, b are the adjustment coefficients of the original Blaney-Criddle equation depending on the air humidity, the hours of actual sunshine and the wind speed. In this case, the values -2.15, 1.38 are chosen for the coefficients a, b, respectively. These values are selected for moderate relative humidity conditions during the day (20–50%), for average wind speed conditions, and for theoretical to actual sunshine ratio between 0.6 and 0.8 (Ponce, 989). The mean daily percentage of annual daytime hours (p) expresses the percentage (%) of daylight hours each

month in relation to the total daylight hours of the year. This percentage is calculated from the following equation (Blaney & Criddle, 1950):

$$p = \frac{N \times \mu}{365 \times 12} \times 100 \quad (2.3)$$

where:
N – the average astronomical daylight duration related to the latitude of the study area (h); m – the number of days in the month under consideration (d). Finally, the daily ETd is converted to monthly using the formula:

$$ETm = ETd \times \mu \quad (2.4)$$

where:
ETm – the monthly potential evapotranspiration (mm. month^{-1}); μ – the total number of days in the respective month

The HEC-HMS model is calibrated using observed data (e.g., river discharge) to improve the predictability and reliability of the model. The model accuracy is typically based on specific statistics and ratings developed to evaluate various performance criteria, such as accuracy of predicting peak flows, total hydrograph volume, peak flow, time to peak etc., depending on project goals (World Bank Group, 2015). In this research, a set of model parameters is estimated empirically and manually using the HMS model's tool "Calibration Aids". The accuracy and performance of the calibrated model is evaluated by three goodness-of-fit measures, the Nash–Sutcliffe efficiency (NSE) coefficient, the percentage bias error (PBIAS), and the Root Mean Squared Error standard deviation ratio (RMSE Std. Dev.) of observations.

1. Nash-Sutcliffe efficiency (NSE) coefficient (Nash & Sutcliffe, 1970):

$$NSE = 1 - \frac{\sum_{i=1}^{n}\left(Q_i^{sim} - Q_i^{obs}\right)^2}{\sum_{i=1}^{n}\left(Q_i^{obs} - \overline{Q^{obs}}\right)^2} \quad (2.5)$$

where:
Q_i^{obs} and Q_i^{sim} – the observed and simulated discharge value at the i^{th} step, respectively; $\overline{Q^{obs}}$ is the average of the observed discharge values; n – the number of observed/simulated values. The NSE coefficient determines the relative magnitude of the error variance compared to the observed data variance. NSE takes values in range between negative infinity (-∞) and 1; value of 1 indicates a perfect agreement, while negative values indicate very poor agreement. Generally, model calibration can be considered satisfactory if the NSE coefficient is greater than 0.50, while NSE coefficient values greater than 0.75 indicate a very good calibration of the model (Moriasi et al., 2007).

2. Percentage bias error (PBIAS), defined as:

$$PBIAS = \frac{\left|\overline{Q^{sim}} - \overline{Q^{obs}}\right|}{\overline{Q^{sim}}} \times 100 \quad (\%) \quad (2.6)$$

where:
$\overline{Q^{sim}}$ and $\overline{Q^{obs}}$ – the simulated and observed mean discharge, respectively. This measure reflects the model's capability to maintain water balance by reproducing total runoff volume. The lower PBIAS, the better is the model's performance.

3. Root Mean Squared Error standard deviation (RMSE Std. Dev.), given by:

$$RMSE\ Std.\ Dev. = \frac{\sqrt{\sum_{i=1}^{n}\left(Q_i^{obs} - Q_i^{sim}\right)^2}}{\sqrt{\sum_{i=1}^{n}\left(Q_i^{obs} - \overline{Q^{obs}}\right)^2}} \quad (2.7)$$

where:
Q_i^{obs} and Q_i^{sim} – the observed and simulated discharge value at the i^{th} step, respectively; $\overline{Q^{obs}}$ – the average of the observed discharge values, and n is the number of observed/simulated values. RMSE Std. Dev. incorporates the benefits of error index statistics and includes a normalization factor, so that the resulting statistic and reported values can apply to various constituents. RMSE Std. Dev. varies from the optimal value of 0 to a large positive value. Lower values of RMSE Std. Dev. nominate a lower root mean square error normalized by the standard deviation of the observations, which indicates the adequacy of the model simulation (Moriasi et al., 2007).

Table 3 General performance ratings for examining statistics

Performance rating	NSE	PBIAS	RMSE Std. Dev.
Very Good	0.75< NSE ≤1.00	PBIAS <±10%	0.00≤ RMSE Std. Dev. ≤0.50
Good	0.65< NSE ≤0.75	±10%≤ PBIAS <±15%	0.50< RMSE Std. Dev ≤0.60
Satisfactory	0.50< NSE ≤0.65	±15%≤ PBIAS <±25%	0.60< RMSE Std. Dev ≤0.70
Unsatisfactory	NSE ≤0.50	PBIAS ≥±25%	RMSE Std. Dev >0.70

Source: Moriasi et al., 2007

The performance ratings for the three goodness-f-fit measures given by Moriasi et al. (2007) are based on the evaluations and corresponding values reported from individual studies. The ratings are summarized in table 3.

3 Results and discussion

3.1 Calibration of the HEC-HMS model

Calibration of the HEC-HMS model are conducted manually using model's tool "Calibration Aids". Fig. 7 shows comparison of observed and simulated monthly discharge for the calibration period and Table 4 summarizes calibration performance metrics. As observed, the HEC-HMS model calibration succeeded, while it accurately estimates peak discharge and volume. The model performance for river discharge is very good according to NSE and RMSE Std. Dev. and good according to PBIAS measure.

3.2 Calibration and validation of the LARS-WG 6.0 model

Daily precipitation, temperature, and solar radiation data for the period 2003–2020 are used for the LARS-WG 6.0 model calibration. Generated time series from calibrated site is generated from random seeds, and performance of LARS-WG 6.0 is evaluated using the QTest validation option. The QTest compares probability distributions, means, and standard deviations for observed and generated data from LARS-WG 6.0. All statistical tests carried out in Qtest calculate a *p*-value. A very low *p*-value means that the simulated climate is unlikely to be the same as the 'true' climate. The level of *p*-value that is considered significant is subjective and depends on the importance of a very close fit for each application (Semenov & Barrow, 2002).

Evaluation of the LARS-WG 6.0 performance in simulating daily precipitation and temperature data for the Kalloni is presented in Tables 5 and 6. The K-S test was used to compare observed and generated data histograms. Table 5 showcased that simulation of both minimum and maximum temperature was perfect. It can also be noted that the model performed very well fitting for mean precipitation in winter and autumn seasons, while on the other hand, very poor performance was observed for summer period (Jun – Aug). The reason for the poor performance may be attributed to the lack of precipitation recorded in summer and small available database time series for baseline scenario. Semenov and Barrow (2002) have reported that sample size affects the likelihood of a significant *p*-value and the tests are more likely to give a significant result with more data. A small sample size with little observed precipitation data in summer gives little information, as to approach 'true' distribution. Chisanga et al. (2017) also reported a poor performance in precipitation due to the lack of observed data during summer. Furthermore, significant differences between simulated and observed data might be due to LARS-WG smoothing of observed data in order to eliminate random noise (Semenov &

Table 4 Calibration performance measures

	Peak discharge ($m^3.s^{-1}$)	Volume (mm)	Date of peak	NSE	PBIAS	RMSE Std. Dev.
Simulated	1.52	143.27	24/01/2019	0.784	-0.10%	0.46
Observed	1.52	143.27	24/01/2019			

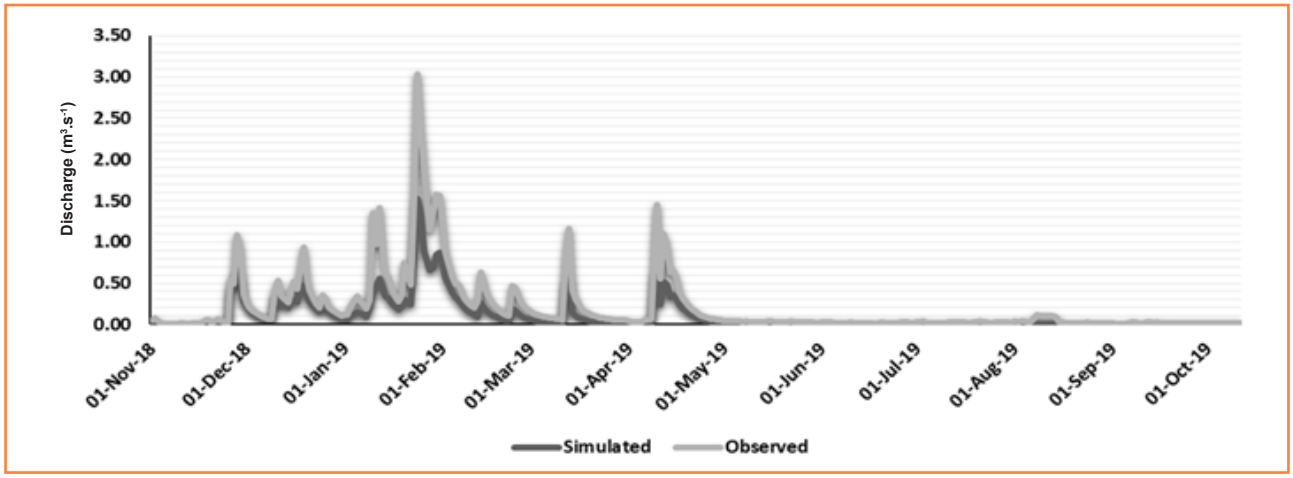


Figure 7 HEC-HMS calibration results for river discharge ($m^3 \cdot s^{-1}$)

Table 5 K-S test for daily precipitation, minimum and maximum temperature distributions

Month	Mean precipitation			Min temperature			Max temperature		
	K-S	*p*-value	assessment	K-S	*p*-value	assessment	K-S	*p*-value	assessment
Jan	0.14	0.97	perfect	0.05	1.00	perfect	0.11	1.00	perfect
Feb	0.05	1.00	perfect	0.11	1.00	perfect	0.05	1.00	perfect
Mar	0.09	1.00	perfect	0.05	1.00	perfect	0.05	1.00	perfect
Apr	0.06	1.00	perfect	0.09	1.00	perfect	0.05	1.00	perfect
May	0.07	1.00	perfect	0.05	1.00	perfect	0.05	1.00	perfect
Jun	0.24	0.49	good	0.05	1.00	perfect	0.05	1.00	perfect
Jul	0.54	0.00	very poor	0.11	1.00	perfect	0.05	1.00	perfect
Aug	0.64	0.00	very poor	0.05	1.00	perfect	0.05	1.00	perfect
Sep	0.15	0.95	perfect	0.05	1.00	perfect	0.05	1.00	perfect
Oct	0.05	1.00	perfect	0.05	1.00	perfect	0.05	1.00	perfect
Nov	0.04	1.00	perfect	0.05	1.00	perfect	0.05	1.00	perfect
Dec	0.03	1.00	perfect	0.11	1.00	perfect	0.05	1.00	perfect

Table 6 Performance results of LARS-WG 6.0 in fitting monthly precipitation and temperature statistics

	R^2	NSE	PBIAS
Mean monthly precipitation	0.983	0.977	5.370
Min monthly temperature	0.997	0.992	2.640
Max monthly temperature	0.997	0.996	0.900

Barrow, 2002). Ebrahim et al. (2012) have also stated that significant difference during winter season is likely due to LARS-WG smoothing for observed data.

Performance of LARS-WG 6.0 is also checked by using coefficient of determinant (R^2), the Nash–Sutcliffe efficiency (NSE) coefficient, and percentage bias error (PBIAS). Table 6 summarized results of analyses of statistical characteristics of observed and generated monthly weather data. R^2 value of 0.99 demonstrates excellent performance of LARS-WG 6.0 in simulating weather variables. Ratings of the Nash-Sutcliffe efficiency coefficient and percentage bias error also showed a very good performance of LARS-WG 6.0 in fitting monthly statistics. Performance of LARS-WG 6.0 in simulating climate variables is demonstrated in Fig. 8 which compares observed and generated average monthly precipitation, and minimum and maximum temperature.

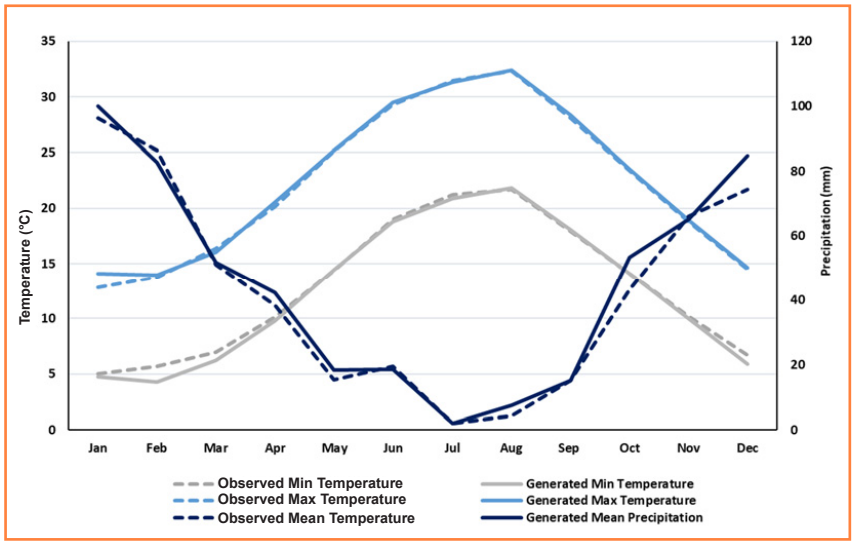


Figure 8 Comparison of LARS-WG 6.0 generated and observed baseline data of mean monthly precipitation, minimum and maximum monthly temperature

3.3 Analysis of precipitation and temperature variables

The first step in analysing effects of climate change on river basin hydrology is to quantify changes in weather variables. Table 7 summarized downscaling results for mean annual precipitation and temperature for various GCMs-RCP

Table 7 Annual changes in precipitation and temperature for all examined GCM-RCP scenarios

Scenario		Annual precipitation (mm)		Temperature (°C)	
GCM	**RCP**	**mean value**	**percent change (%)**	**mean value**	**percent change (%)**
HadGEM2-ES	2.6	529.49	5.36%	18.82	7.59%
EC-EARTH	4.5	537.59	6.97%	18.24	4.23%
GFDL-CM3	4.5	504.90	0.47%	19.25	10.01%
HadGEM2-ES	4.5	543.42	8.13%	19.00	8.63%
MIROC5	4.5	546.65	8.77%	18.83	7.63%
MPI-ESM-MR	4.5	548.50	9.14%	18.29	4.54%
EC-EARTH	8.5	525.75	4.61%	18.83	7.62%
GFDL-CM3	8.5	473.44	-5.79%	20.12	15.03%
HadGEM2-ES	8.5	517.97	3.07%	19.51	11.51%
MIROC5	8.5	537.67	6.99%	19.28	10.18%
MPI-ESM-MR	8.5	536.96	6.84%	18.66	6.63%
Baseline BaU		502.56	0.00%	17.50	0.00%

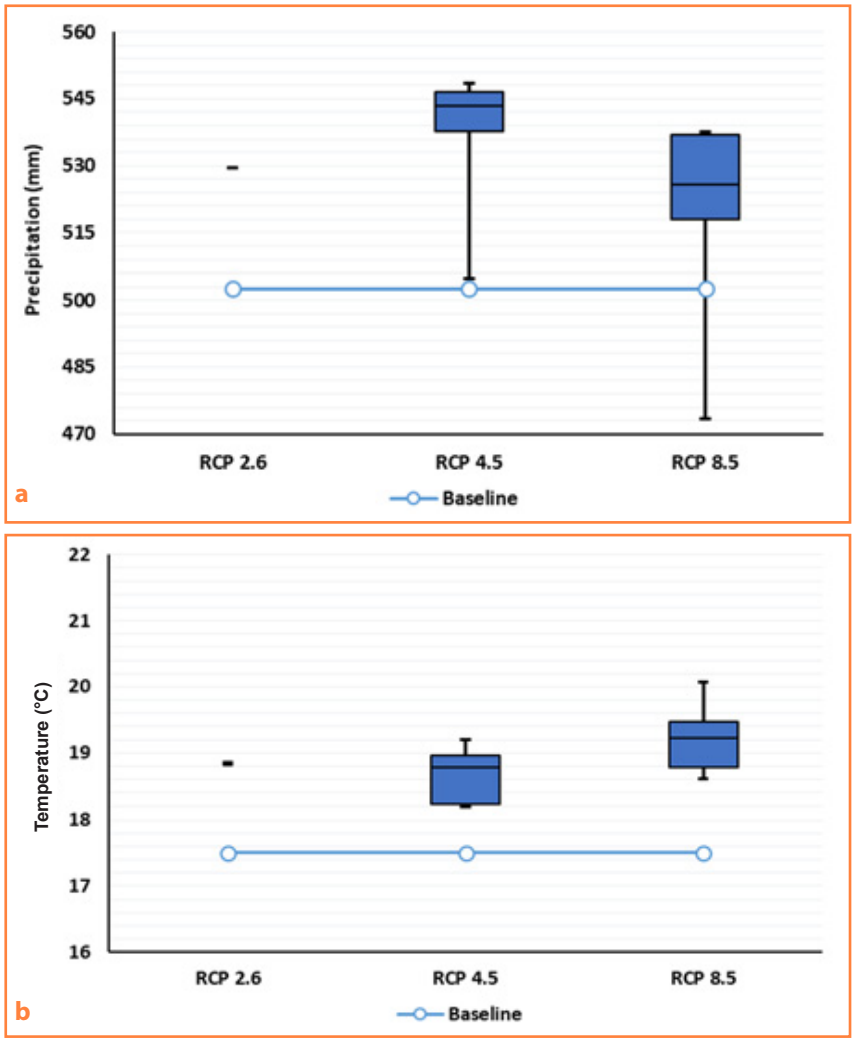


Figure 9 Variations in future (a) mean annual precipitation and (b) mean annual temperature forecasts compared to baseline scenario under the influence of each emissions scenario

scenarios as well as percentage changes of these parameters compared to baseline scenario. The results show a consistently increasing trend both in precipitation and temperature values for all climate models except GFDL-CM3 which shows a reduction of future rainfall by 5.79%. Table 7 also shows a large divergence in changes of annual rainfall totals which range from -5.79% (GFDL-CM3) to +6.99% (MIROC5) for RCP 8.5 and from +0.47% (GFDL-CM3) to +9.14% (MPI-ESM-MR) for RCP 4.5. The annual rate of changes of mean temperature at the Kalloni river basin also range from +6.63% (MPI-ESM-MR) to +15.03% (GFDL-CM3) for RCP 8.5 and +4.23% (EC-EARTH) to +10.01% (GFDL-CM3) for RCP 4.5.

Variations in GCMs outputs concerning predicted annual rainfall totals and average temperatures for future simulation period 2021–2080 are shown as boxplots in Figs 9a and 9b, respectively. The boxplots represent 25th, 50th (median) and 75th percentiles, and horizontal lines show mean annual values for Baseline Business as Usual (BaU) scenario. The generated data from Baseline BaU scenario for the period

2021–2080 match site statistics based on historical records without taking into account climate change. Variations in GCMs result indicate the range of uncertainty in GCM predictions and they arise mainly from wide rainfall patterns generated by different climate models (Hajian et al., 2016; Bates et al., 2008). Therefore, studies investigating the potential effects of climate change on water resources using outflows from a single GCM greatly reduce the validity and usefulness of the findings (Hajian et al., 2016).

Subsequently, it is important to examine the response of these parameters to climate change in a shorter time scale, as they show significant seasonal fluctuations. Tables 8 and 9 show average seasonal changes in total rainfall and average temperature. Table 8 shows that rainfall varies significantly between different GCMs, whereas Table 9 shows more uniform results for temperature. These variations, as well as the final values of the rainfall and temperature parameters on a monthly basis, are visualized in Figs 10a, b, c and 11a, b, c, respectively. As observed, the average cumulative rainfall shows a downward trend in spring and summer and

Table 8 Seasonal changes in mean precipitation for all simulated GCM-RCP scenarios

Scenario		Seasonal Precipitation (mm)				Seasonal percent change (%)			
GCM	RCP	winter	spring	summer	autumn	winter	spring	summer	autumn
HadGEM2-ES	2.6	267.63	93.15	32.43	137.47	1.12%	5.10%	7.10%	14.37%
EC-EARTH	4.5	274.33	81.09	27.61	155.94	3.65%	-8.51%	-8.82%	29.73%
GFDL-CM3	4.5	266.84	94.61	30.37	86.82	0.82%	6.75%	0.30%	-27.77%
HadGEM2-ES	4.5	275.80	87.46	33.05	148.44	4.21%	-1.32%	9.15%	23.49%
MIROC5	4.5	288.08	88.86	28.56	142.60	8.85%	0.26%	-5.68%	18.64%
MPI-ESM-MR	4.5	279.92	88.85	27.15	153.99	5.77%	0.25%	-10.34%	28.11%
EC-EARTH	8.5	262.57	83.54	28.23	152.74	-0.79%	-5.74%	-6.77%	27.07%
GFDL-CM3	8.5	234.61	91.97	32.50	82.70	-11.35%	3.77%	7.33%	-31.20%
HadGEM2-ES	8.5	267.23	87.66	31.59	132.66	0.97%	-1.09%	4.33%	10.37%
MIROC5	8.5	285.50	87.65	27.93	138.04	7.87%	-1.11%	-7.76%	14.84%
MPI-ESM-MR	8.5	276.69	88.60	25.37	147.62	4.55%	-0.03%	-16.22%	22.81%
Baseline BaU		264.66	88.63	30.28	120.20	0.00%	0.00%	0.00%	0.00%

Table 9 Seasonal changes in mean temperature for all simulated GCM-RCP scenarios

Scenario		Mean seasonal temperature (oC)				Seasonal percent change (%)			
GCM	RCP	winter	spring	summer	autumn	winter	spring	summer	autumn
HadGEM2-ES	2.6	10.89	17.00	27.19	20.04	12.53%	9.14%	5.18%	7.11%
EC-EARTH	4.5	10.35	16.32	26.63	19.47	6.89%	4.73%	3.04%	4.10%
GFDL-CM3	4.5	10.78	17.14	28.25	20.60	11.40%	10.01%	9.30%	10.10%
HadGEM2-ES	4.5	10.94	17.14	27.46	20.30	12.98%	10.03%	6.25%	8.50%
MIROC5	4.5	10.78	16.81	27.38	20.18	11.33%	7.87%	5.92%	7.86%
MPI-ESM-MR	4.5	10.35	16.47	26.81	19.35	6.96%	5.72%	3.71%	3.45%
EC-EARTH	8.5	10.97	16.93	27.18	20.06	13.36%	8.66%	5.15%	7.22%
GFDL-CM3	8.5	11.67	17.92	29.21	21.50	20.59%	15.00%	13.00%	14.93%
HadGEM2-ES	8.5	11.34	17.56	28.08	20.88	17.18%	12.71%	8.63%	11.60%
MIROC5	8.5	11.10	17.16	27.96	20.70	14.63%	10.16%	8.18%	10.67%
MPI-ESM-MR	8.5	10.48	16.72	27.35	19.89	8.23%	7.33%	5.83%	6.32%
Baseline BaU		9.68	15.58	25.85	18.71	0.00%	0.00%	0.00%	0.00%

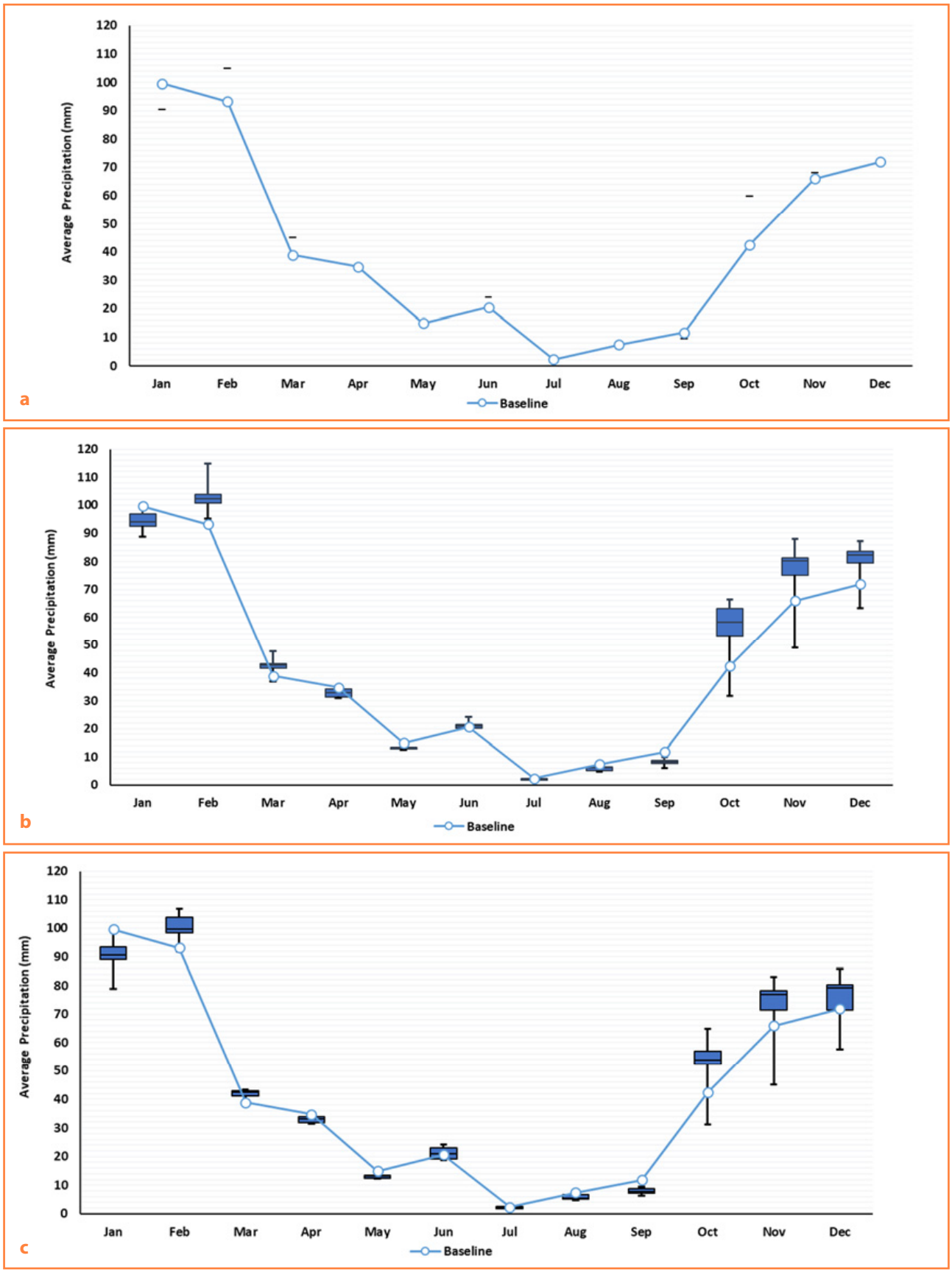


Figure 10 Variations in monthly precipitation forecasts compared to baseline BaU scenario under the influence of each emissions scenario (a) RCP 2.6, (b) RCP 4.5, and (c) RCP 8.5

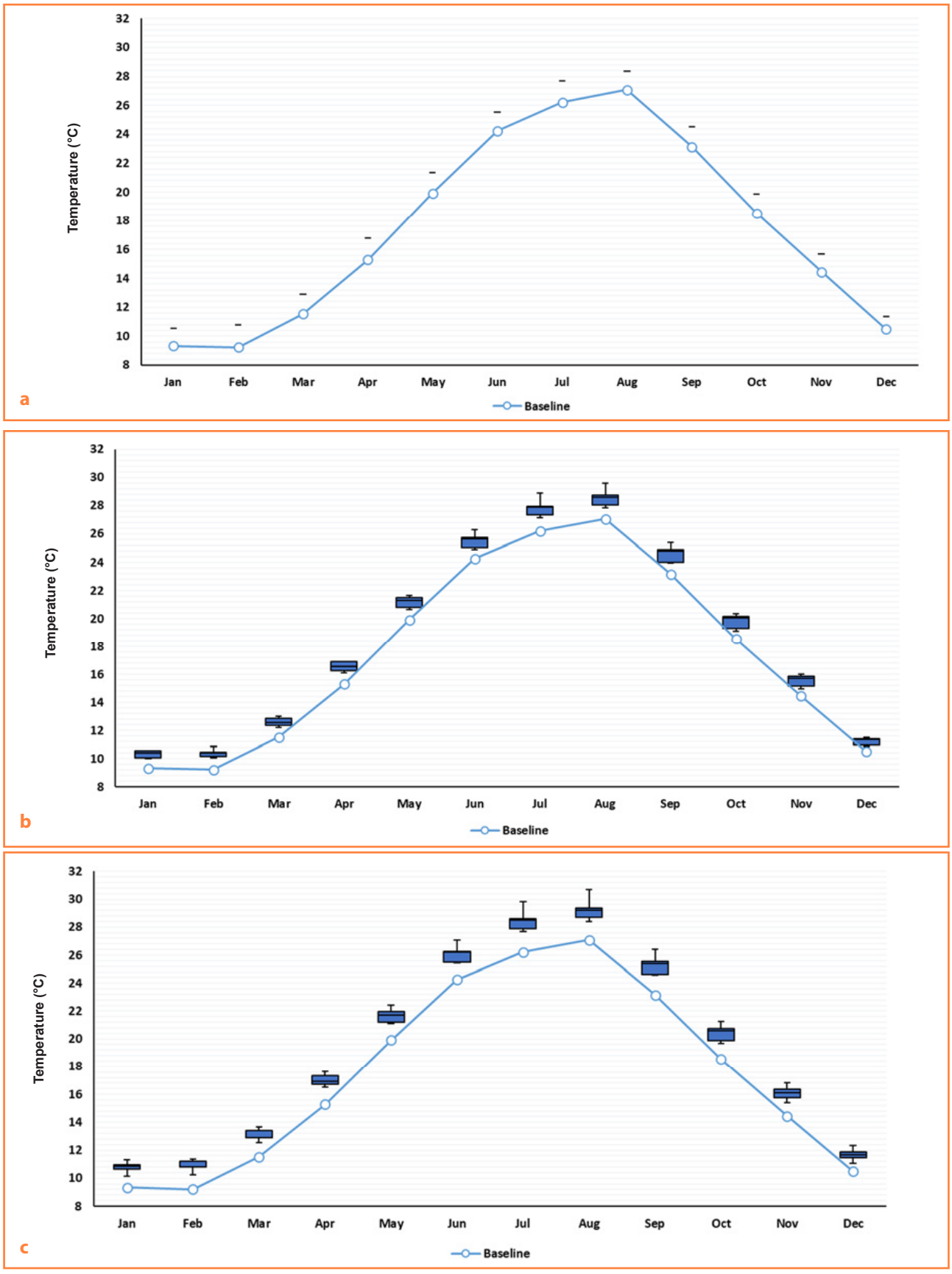


Figure 11 Variations in monthly temperature forecasts compared to baseline BaU scenario under the influence of each emissions scenario (a) RCP 2.6, (b) RCP 4.5, and (c) RCP 8.5

a particularly upward trend in winter and especially autumn. Moreover, there is a shift of peak rainfall from January to February, while January shows a drop in cumulative rainfall. Finally, in terms of temperature, there is a general increase in average temperature throughout the year, while the largest changes occur during the winter months.

3.4 Climate change impact on evapotranspiration

Monthly potential evapotranspiration is computed using the modified Blaney-Criddle method (Blaney & Criddle, 1950) with projected temperature data for 2021–2080 period. Evapotranspiration under various GSMs-RCP scenarios is compared to corresponding baseline Business as Usual (BaU) scenario and percentage changes are summarized in Table 10. Overall results indicate an increase in seasonal evapotranspiration in the region, with significant changes for instance of 7.42%, 7.07%, 7.77% and 7.78% for winter, spring, summer and autumn, respectively, occurring in GFDL-CM3 model for RCP 8.5 emission scenario. Variations in monthly evapotranspiration for all scenarios are represented in Figs 12a, 12b and 12c.

3.5 Climate change impact on streamflow

Annual peak and average monthly river discharges are computed using the calibrated HEC-HMS model based on projected weather data for 2021–2080 period. Figs 13a, b, c and 14a, b, c show annual peak and seasonal discharge variations respectively, under all examined GCM models for three RCP scenarios. Although the results from different scenarios vary considerably, a general increasing trend of flow peaks is observed, especially during the long-term period 2040–2080. In terms of monthly variations, January presents highest peaks in all scenarios as well

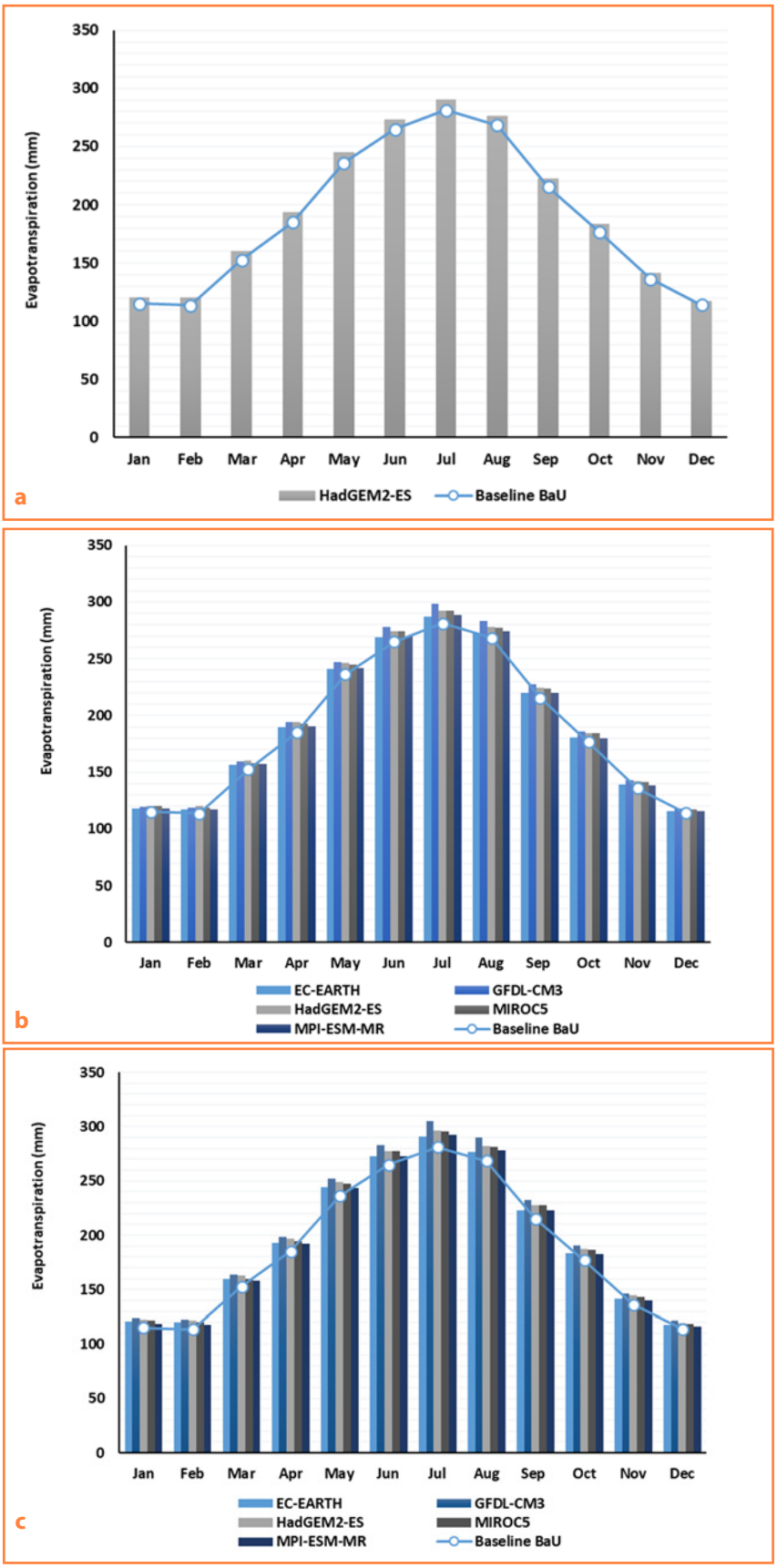


Figure 12 Monthly evapotranspiration variations under all examined GCM models for (a) RCP2.6, (b) RCP4.5, and (c) RCP8.5 scenarios

Table 10 Seasonal changes in evapotranspiration for all examined GCM-RCP scenarios

Scenario		Seasonal Evapotranspiration (mm)				Seasonal percent change (%)			
GCM	**RCP**	**winter**	**spring**	**summer**	**autumn**	**winter**	**spring**	**summer**	**autumn**
HadGEM2-ES	2.6	119.35	199.50	279.98	182.56	4.53%	4.29%	3.10%	3.68%
EC-EARTH	4.5	117.03	195.55	276.50	179.82	2.49%	2.22%	1.82%	2.12%
GFDL-CM3	4.5	118.87	200.36	286.64	185.36	4.11%	4.73%	5.56%	5.27%
HadGEM2-ES	4.5	119.54	200.32	281.71	183.86	4.69%	4.71%	3.74%	4.41%
MIROC5	4.5	118.85	198.42	281.17	183.28	4.09%	3.72%	3.54%	4.09%
MPI-ESM-MR	4.5	117.06	196.44	277.58	179.27	2.52%	2.69%	2.22%	1.81%
EC-EARTH	8.5	119.69	199.05	279.91	182.65	4.82%	4.05%	3.08%	3.73%
GFDL-CM3	8.5	122.65	204.82	292.64	189.78	7.42%	7.07%	7.77%	7.78%
HadGEM2-ES	8.5	121.26	202.73	285.56	186.68	6.20%	5.98%	5.16%	6.02%
MIROC5	8.5	120.21	200.50	284.83	185.87	5.28%	4.81%	4.89%	5.56%
MPI-ESM-MR	8.5	117.58	197.91	281.02	181.91	2.97%	3.45%	3.48%	3.31%
Baseline BaU		114.18	191.30	271.55	176.08	0.00%	0.00%	0.00%	0.00%

Table 11 Annual changes in river discharge for all examined GCM-RCP scenarios

Scenario		Annual discharge ($m^3.s^{-1}$)		Annual percent change (%)	
GCM	**RCP**	**peak**	**average**	**peak**	**average**
HadGEM2-ES	2.6	4.24	1.34	-5.57%	16.86%
EC-EARTH	4.5	4.79	1.56	6.68%	36.50%
GFDL-CM3	4.5	4.70	1.37	4.68%	19.49%
HadGEM2-ES	4.5	4.70	1.48	4.68%	29.26%
MIROC5	4.5	5.02	1.58	11.80%	38.23%
MPI-ESM-MR	4.5	4.76	1.60	6.01%	39.60%
EC-EARTH	8.5	4.70	1.44	4.68%	25.84%
GFDL-CM3	8.5	4.70	1.34	4.68%	16.74%
HadGEM2-ES	8.5	4.55	1.26	1.34%	10.13%
MIROC5	8.5	4.92	1.51	9.58%	32.22%
MPI-ESM-MR	8.5	4.53	1.53	0.89%	33.69%
Baseline BaU		4.49	1.14	0.00%	0.00%

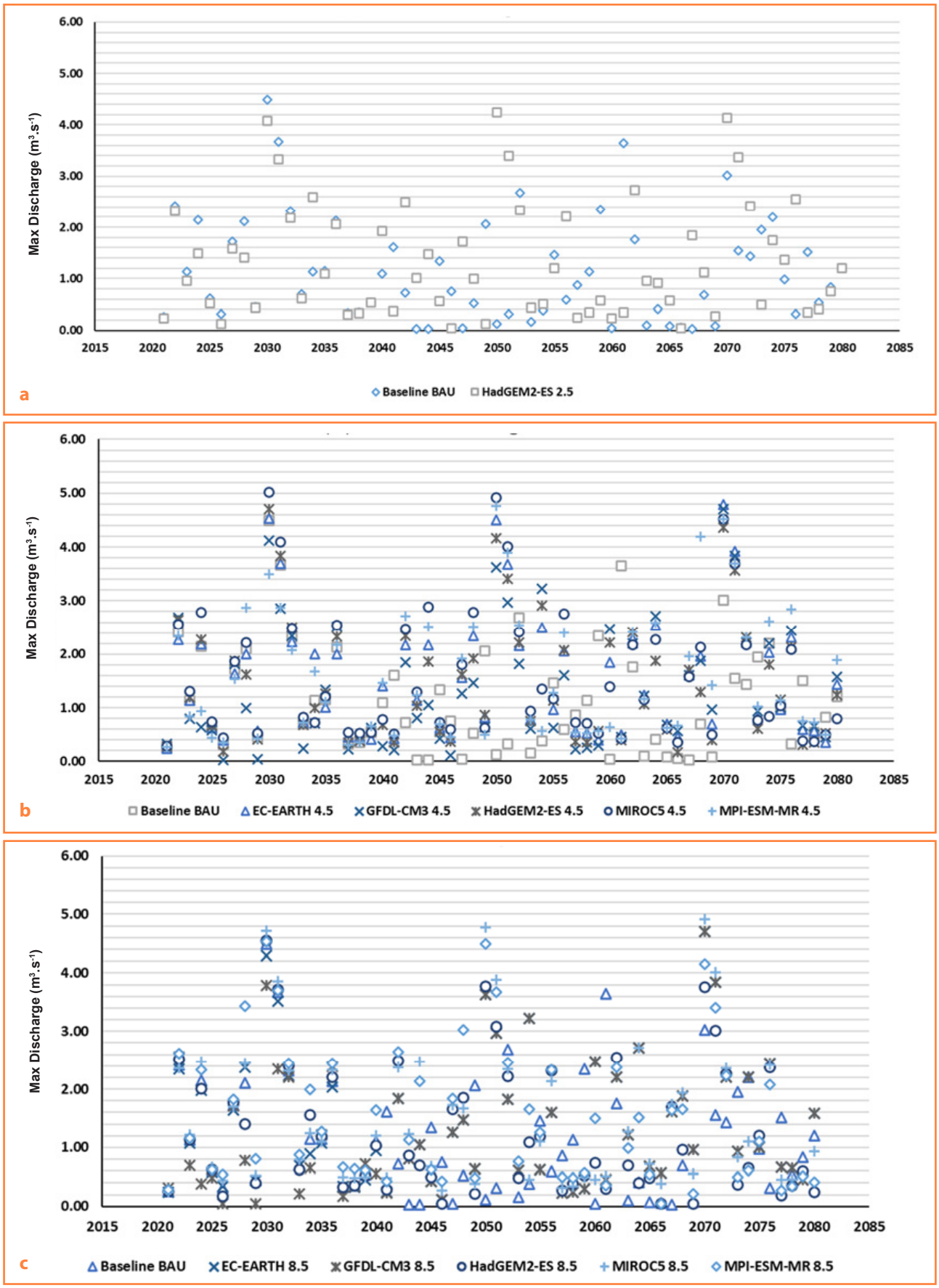


Figure 13 Annual peak discharge variations under all examined GCM models for (a) RCP2.6, (b) RCP4.5, and (c) RCP8.5 scenarios

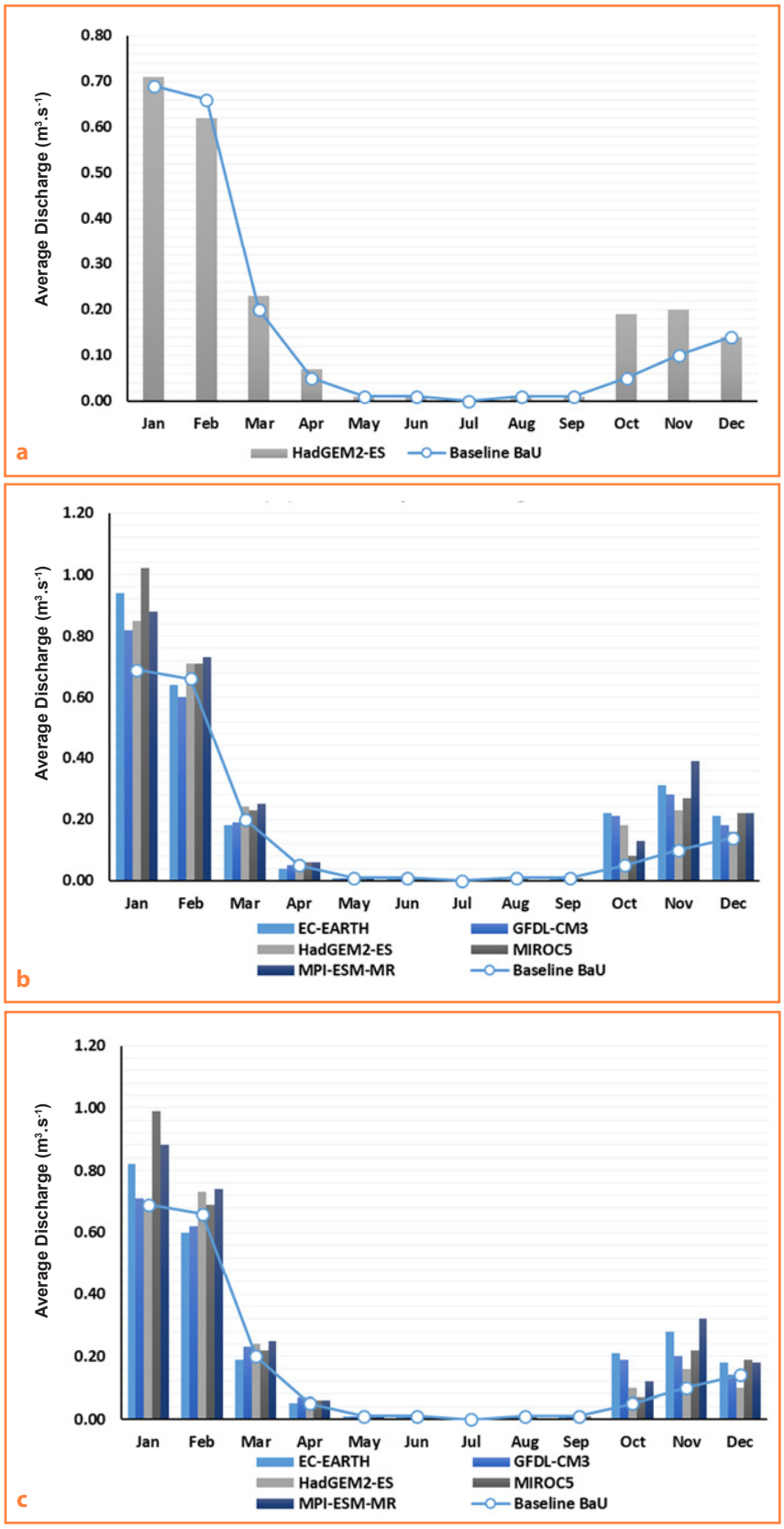


Figure 14 Monthly discharge variations under all examined GCM models for (a) RCP2.6, (b) RCP4.5, and (c) RCP8.5 scenarios

as in baseline scenario. However, the most critical months are October and November, which show more than double discharge compared to the baseline scenario. Also, in future, dry months August and September are expected to have even lower discharges. This sudden surge of streamflow from summer to autumn months is of particular concern as it increases the risk of flash floods occurrence.

Table 11 summarizes percent difference in annual average and peak discharge between baseline BaU scenario and each of future scenarios considered. It is observed that average discharge is increasing rapidly in future, with the most "optimistic" scenario being for HadGEM2-ES model and RCP8.5 (+10.13% increase) and the most "pessimistic" scenario being for MPI-ESM-MR model and RCP4.5 (+39.60% increase). On the other hand, annual peak discharge showed smaller changes, which vary from -5.75% decrease for HadGEM2-ES model and RCP8.5 to +11.80% increase for MIROC5 model and RCP4.5. Moreover, Table 12 summarizes seasonal changes in discharge as percentages of the mean values. Autumn shows the most significant expected increase in discharge as noted above, whereas summer and spring are the seasons with the largest number of discharge reductions. Finally, although winter is the season with the highest discharge amounts, it presents the smallest future percentage changes under climate change scenarios.

Table 12 Seasonal changes in river discharge for all examined GCM-RCP scenarios

Scenario		Seasonal discharge ($m^3.s^{-1}$)				Seasonal percent change (%)			
GCM	RCP	**winter**	**spring**	**summer**	**autumn**	**winter**	**spring**	**summer**	**autumn**
HadGEM2-ES	2.6	0.49	0.10	0.01	0.13	-1.34%	19.23%	0.00%	150.00%
EC-EARTH	4.5	0.60	0.08	0.00	0.18	20.13%	-11.54%	-50.00%	237.50%
GFDL-CM3	4.5	0.53	0.08	0.00	0.17	7.38%	-3.85%	-50.00%	212.50%
HadGEM2-ES	4.5	0.57	0.10	0.01	0.14	15.44%	15.38%	0.00%	162.50%
MIROC5	4.5	0.65	0.10	0.01	0.12	30.87%	15.38%	0.00%	125.00%
MPI-ESM-MR	4.5	0.61	0.11	0.00	0.17	22.82%	23.08%	-50.00%	225.00%
EC-EARTH	8.5	0.53	0.08	0.00	0.17	7.38%	-3.85%	-50.00%	212.50%
GFDL-CM3	8.5	0.49	0.10	0.01	0.13	-1.34%	19.23%	0.00%	150.00%
HadGEM2-ES	8.5	0.50	0.10	0.01	0.09	1.34%	15.38%	0.00%	62.50%
MIROC5	8.5	0.62	0.10	0.01	0.10	25.50%	11.54%	0.00%	87.50%
MPI-ESM-MR	8.5	0.60	0.11	0.00	0.15	20.81%	23.08%	-50.00%	175.00%
Baseline BaU		0.50	0.09	0.01	0.05	0.00%	0.00%	0.00%	0.00%

4 Conclusions

The present study investigates the climate change impact on hydrologic regime of the Kalloni river basin with intermittent flow in response to different climatic models and conditions. The LARS-WG version 6.0 was used along with five GCM models and three emission scenarios to generate climatic variables. In total, eleven sets of GCM-RCP scenarios were considered when predicting future rainfall, temperatures, and radiation patterns, covering a wide range of uncertainties. Hydrological model simulations were conducted for the baseline climate and each of the climate scenarios in the environment of HEC-HMS version 4.3. The results obtained demonstrate that the approach combining hydrological model HEC-HMS and LARS-WG weather generator is efficient for assessing the effects of climate change on the patterns of the river hydrology.

Annual and seasonal predictions of weather variables, evapotranspiration, and discharge for the Kalloni river basin were obtained based on various GCMs and RCPs scenarios for assessing climate change impact on hydrologic regime of the basin. Overall findings indicate an increase in mean annual rainfall and temperature for the region. In seasonal patterns, a significant increase in precipitation is expected in autumn. Slight increase or even decrease can be anticipated in summer and spring rainfall totals. A general increasing trend of mean temperature and a consequent change in evapotranspiration was observed throughout the year, with the most significant change occurring in winter. The projected decrease in summer precipitation and higher evapotranspiration are expected to cause a reduction in soil water and groundwater recharge in the basin area. This reduction in summer combined with the tremendous increase in autumn discharge leads to a high risk of flooding, particularly in the form of flash floods. Such findings indicate the need for integrated water management and flood mitigation strategies in the area of the Kalloni river basin.

This paper provides a quantitative framework for policymakers in small, intermittent flow, river basins in the Mediterranean, such as the Kalloni, to plan and manage the expected future challenges of river discharge and flood occurrence.

Acknowledgments

This research equipment's installation and operational cost was funded partly by the National Strategic Reference Framework (NSRF) 2014–2020, through the project "Observatory of Coastal Environment – AEGIS" and the ERMIS-flood Interreg project. Thanks are due to M. Champas, A. Gkerekos and G. Exintaris for their help in fieldwork and instrument installation and conservation at the Kalloni River and Professor K. Kalabokidis for the AEGIS-fire laboratory data provision.

References

Ali, M., Khan, S. J., Aslam, I., & Khan, Z. (2011). Simulation of the impacts of land-use change on surface runoff of Lai Nullah Basin in Islamabad, Pakistan. *Landsc. Urban Plan.*, *102*(4), 271–279.

Bai, Y., Zhang, Z., & Zhao, W. (2019). Assessing the Impact of Climate Change on Flood EventsUsing HEC-HMS and CMIP5. *Water Air Soil Pollution*. *230*(119).
https://doi.org/10.1007/s11270-019-4159-0

Bates, B.C. et al. (2008). *Climate change and water.* Technical paper of the Intergovernmental Panel on Climate Change. IPCC Secretariat.

Blaney, H. F., & Criddle, W. D. (1950). *Determining water requirements in irrigated areas from climatological and irrigated data.* SCS, TP-96, USDA.

Chisanga, C. B., Phiri, E., & Chinene, V. R. N. (2017). Statistical Downscaling of Precipitation and Temperature Using Long Ashton Research Station Weather Generator in Zambia: A Case of Mount Makulu Agriculture Research Station. *American Journal of Climate Change*, *6*, 487–512. DOI: 10.4236/ajcc.2017.63025. http://www.scirp.org/journal/ajcc

Cisneros, J. B.E. (2014). Part A: Global and Sectoral Aspects. Contribution of Working Group II to the Fifth Assessment Report of the Intergovernmental Panel on Climate Change. In V.R. Barros, C.B. Field, D.J. Dokken, M.D. Mastrandrea, K.J. Mach, T.E. Bilir, M. Chatterjee, K.L. Ebi, Y.O. Estrada, O.C. Genova, et al. Eds., *Climate Change 2014: Impacts, Adaptation, and Vulnerability* (pp. 229–269). Cambridge University Press.

Doorenbos, J., & Pruitt, W.O. (1977). *Crop water requirements* (Irrigation and Drainage Paper No. 24, 144 p.). FAO, United Nations.

Ebrahim, G. Y., Jonoski, A., van Griensven, A., & Di Baldassarre, G. (2012). Downscaling technique uncertainty in assessing hydrological impact of climate change in the Upper Beles River Basin, Ethiopia. *Hydrology Research, 44*(2)*, 377–398.* doi: 10.2166/nh.2012.037.

Emam, A. R., Mishra, B. K., Kumar, P., Masago, Y., & Fukushi, K. (2016). Impact Assessment of Climate and Land-Use Changes on Flooding Behavior in the Upper Ciliwung River, Jakarta, Indonesia. *Water*, *8*, 559. doi:10.3390/w8120559.

European Environmental Agency.
https://www.eea.europa.eu/data-and-maps/data/eu-dem

Hajian, F., Dykes, A. P., Zahabiyoun, B., & Ibsen, M. (2016). Prediction of climate change effects on the runoff regime of a forested basin in northern Iran. *Hydrological Sciences Journal*, *61*(15), 2729–2739. DOI: 10.1080/02626667.2016.1171870.

Hewer, M. J. & Gough, W.A. (2018). Thirty years of assessing the impacts of climate change on outdoor recreation and tourism in Canada. *Tour Manag Perspect, 26*,179–192. https://doi.org/10.1016/j.tmp.2017.07.003

HMSO. (1962). *Weather in the Mediterranean I: general meteorology* (2nd ed.). Her Majesty's Stationery Office.

Intergovernmental Panel on Climate Change (IPCC). (2000). *IPCC Special Report Emissions Scenarios*. Intergovernmental Panel on Climate Change, Working Group III. IPCC.

Intergovernmental Panel on Climate Change (IPCC). (2014). In R.K. Pachauri, L.A. Meyer (Eds.), *Climate Change 2014: Synthesis Report*. Core Writing Team, Contribution of Working Groups I, II and III to the Fifth Assessment Report of the Intergovernmental Panel on Climate Change. IPCC.

Ismail, H., Kamal, Md. R., Abdullah, A. F. B., Jada, D. T., & Hin, L. S. (2020). Modeling Future Streamflow for Adaptive Water Allocation under Climate Change for the Tanjung Karang Rice Irrigation Scheme Malaysia. *Applied Sciences*, *10*(14), 4885. doi:10.3390/app10144885.

Lavell, A., M. Oppenheimer, C. Diop, J. Hess, R. Lempert, J. Li, R. Muir-Wood, & Myeong, S. (2012). Climate change: new dimensions in disaster risk, exposure, vulnerability, and resilience. In C.B. Field, V. Barros, T.F. Stocker, D. Qin, D.J. Dokken, K.L. Ebi, M.D. Mastrandrea, K.J. Mach, G.-K. Plattner, S.K. Allen, M. Tignor, & P.M. Midgley (eds.), *Managing the Risks of Extreme Events and Disasters to Advance Climate Change Adaptation* (pp. 25–64). A Special Report of Working Groups I and II of the Intergovernmental Panel on Climate Change (IPCC). Cambridge University Press.

Manfreda, S. (2018). On the derivation of flow rating curves in data-scarce environments. *Journal of Hydrology, 562,* 151–154. DOI: 10.1016/j.jhydrol.2018.04.058.
https://doi.org/10.1016/j.jhydrol.2018.04.058

Matrai, I., & Tzoraki, O. (2018). Assessing stakeholder perceptions regarding floods in Kalloni and Agia Paraskevi, Lesvos Greece. *HYDROMEDIT Conference*, 818–820.

Meenu, R., Rehana, S., & Mujumdar, P. P. (2012). Assessment of hydrologic impacts of climate change in Tunga – Bhadra river basin, India with HEC-HMS and SDSM. *Hydrological prosesses*. DOI: 10.1002/hyp.9220.

Moriasi, D.N., Arnold, J.G., Van Liew, M.W., Bingner, R.L., Harmel, R.D. & Veith, T.L. (2007). Model evaluation guidelines for systematic quantification of accuracy in watershed simulations, *Trans. Am. Soc. Agric. and Biol. Eng*., *50*(3), 885−900.

Nash, J. E., & Sutcliffe, J. V. (1970). River flow forecasting through conceptual models part I: A discussion of principles. *Journal of Hydrology*, *10*(3), 282–290.

Nourani, V, Baghanam, A.H., & Gokcekus, H. (2018). Data-driven ensemble model to statistically downscale rainfall using nonlinear predictor screening approach. *J Hydrol, 565*,538–551. https://doi.org/10.1016/j.jhydrol.2018.08.049

Nyaupane, N., Mote, S. R., Bhandari, B., & Kalra, A. (2018). Rainfall-Runoff Simulation Using Climate Change Based Precipitation Prediction in HEC-HMS Model for Irwin Creek, Charlotte, North Carolina. *World Environmental and Water Resources Congress*.

Parry, M.L., Canziani, O.F., Palutikof, J.P., van der Linden, P.J., & Hanson, C.E. (Eds.) (2007). *Climate Change 2007: Impacts, Adaptation and Vulnerability.* Contribution of Working Group II to the Fourth Assessment Report of the Intergovernmental Panel on Climate Change, Cambridge University Press.

Ponce, V. M. (1989). *Engineering Hydrology, Principles and Practices*.

Qin, X. S., & Lu, Y. (2014). Study of Climate Change Impact on Flood Frequencies: A Combined Weather Generator and Hydrological Modeling Approach. *Journal of hydrometeorology*, *15*(3), 1205–1219. DOI: 10.1175/JHM-D-13-0126.1

Racsko, P., Szeidl, L., & Semenov, M. (1991). A serial approach to local stochastic weather models. *Ecol Model, 57*, 27–41. https://doi.org/10.1016/0304-3800(91)90053-4

Randall, D.A., Wood, R.A., Bony, S., Colman, R., Fichefet, T., Fyfe, J., Kattsov, V., Pitman, A., Shukla, J., Srinivasan, J., Stouffer, R.J., Sumi, A., & Taylor, K.E. (2007). Cilmate Models and Their Evaluation. In S. Solomon, D. Qin, M. Manning, Z. Chen, M. Marquis, K.B. Averyt, M.Tignor, H.L. Miller (Eds.), *Climate Change 2007: The Physical Science Basis*. Contribution of Working Group I to the Fourth Assessment Report of the Intergovernmental Panel on Climate Change. Cambridge University Press.

Refsgaard, J.C., Arnbjerg-Nielsen, K., & Drews, M., et al. (2013). The role of uncertainty in climate change adaptation

strategies – A Danish water management example. *Mitig Adapt Strateg Glob Change, 18*, 337–359. https://doi.org/10.1007/s11027-012-9366-6

Sharma, D., Gupta, A.D., & Babel, M.S. (2007). Spatial disaggregation of bias-corrected GCM precipitation for improved hydrologic simulation: Ping River Basin, Thailand. *Hydrology and Earth System Sciences*, *11*, 1373–1390. www.hydrol-earth-syst-sci.net/11/1373/2007/

Scharffenberg, W., Ely, P., Daly, S., Fleming, M., & Pak, J. (2010). Hydrologic Modeling System (HEC-HMS): Physically-Based Simulation Components. *2nd Joint Federal Interagency Conference,* Las Vegas, NV.

Semenov, M. A., & Barrow, E. M. (2002). LARS-WG – *A Stochastic Weather Generator for Use in Climate Impact Studies*. User Manual, Version 3.0

Semenov, M.A., & Barrow, E.M. (1997). Use of a stochastic weather generator in the development of climate change scenarios. *Clim. Chang., 35*, 397–414.

Sharafati, A., Pezeshki, E., Shahid, S., & Motta, D. (2020). Quantification and uncertainty of the impact of climate change on river discharge and sediment yield in the Dehbar river basin in Iran. *Journal of Soils and Sediments*, *20*, 2977–2996. https://doi.org/10.1007/s11368-020-02632-0

Shrestha, A., Babel, M. S., Weesakul, S., & Vojinovic, Z. (2017). Developing Intensity – Duration – Frequency (IDF) Curves under Climate Change Uncertainty: The Case of Bangkok, Thailand. *Water, 9*(145). doi:10.3390/w9020145

Sunyer, M.A., Madsen, H., & Ang, P.H. (2012). A comparison of different regional climate models and statistical downscaling methods for extreme rainfall estimation under climate change. *Atmos. Res., 103*, 119–128.

Tzoraki, O. (2020). Operating Small Hydropower Plants in Greece under Intermittent Flow Uncertainty: The Case of Tsiknias River (Lesvos). *Challenges*, *11*(17), doi:10.3390/challe11020017.

U.S. Army Corps of Engineers (USACE). (2013). *HEC-GeoHMS Geospatial Hydrologic Modeling Extension*. Hydrologic Engineering Center, User's Manual, Version 10.1.

U.S. Army Corps of Engineers (USACE). (2018). *Hydrologic Modeling System, HEC-HMS*. Hydrologic Engineering Center, User's Manual, Version 4.3.

Verma, A. K., Jha, M. K., & Mahana, R. K. (2010). Evaluation of HEC-HMS and WEPP for simulating watershed runoff using remote sensing and geographical information system. *Paddy Water Environ.*, *8*(2), 131–144.

Wang, M., Zhang, L., & Baddoo, T. D. (2016). Hydrological Modeling in A Semi-Arid Region Using HEC-HMS. *Journal of Water Resource and Hydraulic Engineering*. DOI: 10.5963/JWRHE0503004.

Westerberg, I., Guerrero, J.-L., Seibert, J., Beven, K.J., & Halldin, S. (2011). Stage-discharge uncertainty derived with a non-stationary rating curve in the Choluteca River. *Hydrol. Process*, *25*, 603–613. 10.1002/hyp.7848.

Wilby, R., Dawson, C., & Barrow, E. (2002). SDSM – A decision support tool for the assessment of regional climate change impacts. *Environ. Model. Softw., 17*, 145–157.

Wilks, D.S., & Wilby, R.L. (1999). The weather generation game: A review of stochastic weather models. *Prog. Phys. Geogr., 23*, 329–357.

World Bank Group. (2015). *Water and Climate Adaptation Plan for the Sava River Basin*. ANNEX 1 – Development of the Hydrologic Model for the Sava River Basin.

Wu, C.H., Huang, G.R., & Yu, H.J. (2015). Prediction of extreme floods based on CMIP5 climate models: a case study in the Beijiang River basin, South China. *Hydrology and Earth System Sciences*, *19*(3), 1385–1399.

Yilmaz, A. G. & Imteaz, M. A. (2011). Impact of climate change on runoff in the upper part of the Euphrates basin. *Hydrological Sciences Journal – Journal des Sciences Hydrologiques*, *56*(7), 1265–1279. DOI:10.1080/02626667.2011.609173.

Zhai, P., Pörtner, H.O., & Roberts, D. (2018) Summary for policymakers. In *Global Warming of 1.5 C. An IPCC Special Report on the Impacts of Global Warming of 1.5 C above Pre-Industrial Levels and Related Global Greenhouse Gas Emission Pathways*, p. 32. IPCC.